AT&T Technical Journal
Vol. 64, No. 7, September 1985
Printed in U.S.A.

Simple Analytical Representation of Antenna Spatial Radiation Patterns With Application to the Pyramidal Horn-Reflector Antenna

By J. SHAPIRA*

(Manuscript received January 14, 1985)

The spatial (three-dimensional) radiation characteristics of directive antennas are often needed in radio interference calculations and predictions. Presented is a method that allows a fast computation of the spatial radiation envelope characteristics of antennas from measured pattern information. This is achieved by fitting the measured data to simple functional forms that are based on salient physical properties of the antennas. An example is given in which radiation envelopes for a pyramidal horn-reflector antenna, widely used in AT&T service, are calculated from measured data. Superpositions of quadratic functions to fit main radiation lobes and logarithmic functions to represent the side-lobe envelopes are being used, and good agreement with the measured data is demonstrated.

I. INTRODUCTION

Ground scattering is a major source of interference in microwave communication links.[1] Its analysis involves repeated computations incorporating the antenna directivity in different directions throughout its three-dimensional (3D) coverage.

For a mathematical representation of the 3D directivity pattern of the antenna to be applicable for such purposes, it should be compatible with the data storage and computability constraints and commensurate with the accuracy requirements of the analysis package. Direct

* AT&T Bell Laboratories.

representation of measured data, for instance, requires storage of densely sampled data, about 20 points per beamwidth in every measurement cut, and a fraction of a beamwidth separation between cuts, resulting in the immense number of 400,000 points in the data storage for a 1°-beamwidth antenna. Interpolation methods, based on the bandlimitedness of the antenna spatial spectrum, can reduce the required database by at least two orders of magnitude,[2,3] but many applications require even further simplicity. Such a simplification can be offered by approximating the radiation pattern by its envelope only and disregarding the detailed side-lobe structure, which varies from one antenna unit to another of the same type and varies rapidly with frequency.

The envelope surface, representing a local angular average (or peak cover) of the radiation pattern, is much smoother and more repeatable. Its generation still requires all side-lobe peaks, and any general procedure of surface matching is not as straightforward and simple as desired. A major reduction in complexity may be achieved when use is made of salient features of the antenna. It is demonstrated, in what follows, that a complex surface may be well approximated to a high degree of accuracy with relatively simple analytic expressions by relying on basic antenna features.

It is worth mentioning here that simple models, using a single skirt function, have found use for specifications,[4,5] but their approximation is much too crude for other applications.

The approximation to the radiation pattern of the Pyramidal Horn-Reflector (PHR) antenna,[6] widely used by AT&T Communications, is worked out as an example encompassing only four coefficients in each region, out of a lookup table with 29 constants, while maintaining tight match over the main beam and no more than 5-dB deviation from the side-lobe peaks throughout. This work was briefly summarized in Ref. 7.

II. SURVEY OF PERTINENT ANTENNA FEATURES

2.1 Symmetries in the antenna pattern

The field distribution in a radiating aperture is transformed to the far field via the Fourier Transform (FT),

$$F(u, v) \propto \int_{\text{aperture}} dx \int dy f(x, y) e^{-jk(xu+yv)} \tag{1}$$

(see Fig. 1), where

$$u = \sin\theta \sin\phi$$
$$v = \sin\theta \cos\phi,$$

and k, being the wave number, equals $(2\pi)/\lambda$.

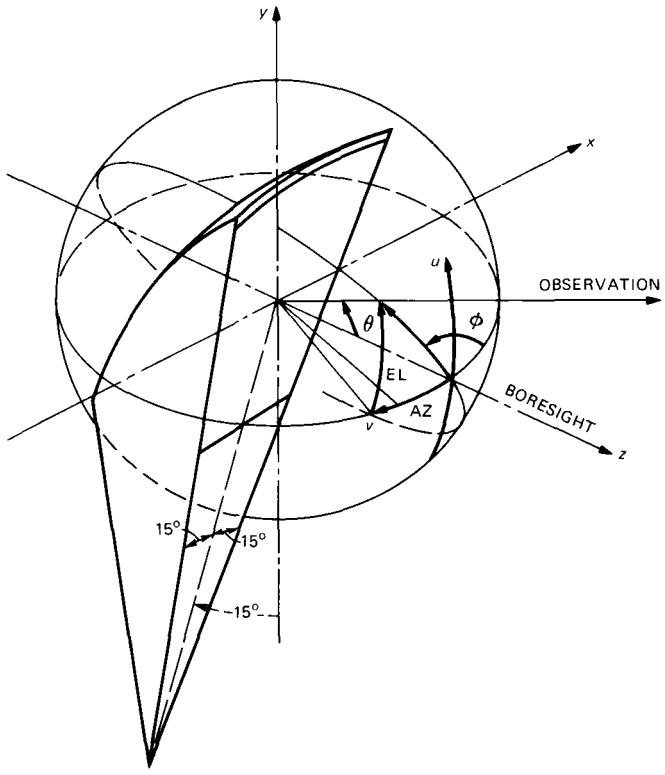

Fig. 1—Coordinate systems for the pyramidal horn-reflector antenna.

For any cut through the z axis (perpendicular to the aperture), one may rotate the coordinates to align the cut with the u and v axes and, thus, reduce eq. (1) to a one-dimensional FT

$$F(u, o) \propto \int_{\text{aperture}} dx e^{-jkxu} \int_{\text{aperture}} dy f(x, y), \tag{2}$$

where the symmetry rules of Table I apply.

The aperture of the PHR antenna, for example, is tilted and not perpendicular to its main beam boresight (see Fig. 1). In the vertical plane, the aperture distribution is, therefore, not real, and the resulting radiation pattern not symmetrical. A simple computation technique by which the field is projected onto a virtual vertical aperture is widely used (see Refs. 8 through 10 in connection with the PHR antenna) and produces a symmetrical pattern in the vertical plane, which is obviously in error. In the horizontal plane, however, the aperture is perpendicular to the pattern boresight and is symmetrical. Further,

Table I—Aperture symmetry rules

Rule	Aperture Distribution	Radiation Pattern
1	$f(x)$ real or $f(x) = \lvert f(x)\rvert e^{j\psi(x)}$	$\lvert F(u)\rvert = F\lvert(-u)\rvert$ $\arg F(u) = -\arg F(-iu)$
2	$f(x) = \pm f(-x)$	$F(u) = \pm F(-u)$
3	$f(x, y) = f_x(x)f_y(y)$	$F(u, \theta) = F_u(u)F_v(v)$ $f_x(x) <\!\!\rightarrow F_u(u)$ $f_y <\!\!\rightarrow F_v(v)$
4	$f(\rho, \phi) = f_\rho(\rho)e^{jn\phi}$ $\rho = \sqrt{x^2 + y^2}$ $\phi = tg^{-1}(y/x)$	$F(u, v) = F_n(w)e^{-jn\Phi}$ $w = \sqrt{u^2 + v^2}$ $\Phi = tg^{-1}(u/v)$ (Hankel transform)

Table II—Asymptotic power density drop-off for rectangular distributions

Rectangular Aperture Distribution	Asymptotic Power Density Drop-Off
Uniform	u^{-2}
Cosine	u^{-4}
$(\text{Cosine})^2$	u^{-6}
$(\text{Cosine})^3$	u^{-8}
Taylor	u^{-2}
Dolph-Chebyshev	Constant

with the side walls of the aperture tilted, the field is not separable (rule 3 in Table I), nor is the far field.

2.2 Asymptotic drop-off of the radiation pattern envelope

The FT relationship between the aperture field and the radiation pattern may be evaluated asymptotically for large u. By integrating by parts one gets

$$F(u) = \int_a^b f(x)e^{-jkxu}dx$$

$$= \sum_{n=0}^{\infty} \left(\frac{1}{u}\right)^{n+1} f^{(n)}(x)e^{-j[kxu+(n-1)\pi/2]}\Big|_a^b, \tag{3}$$

which represents the radiation pattern as an asymptotic series of diffraction terms by discontinuities at the aperture edges. The leading term in that inverse power series is determined by the order of the derivative of the aperture illumination that is discontinuous at the edges. A representative list of aperture distributions, along with the resulting power density drop-off, is listed in Table II (for an extensive list, refer to Ref. 11).

Phase-modulated aperture distributions (e.g., wide flare horns, shaped beam antennas) may have an additional, nondiffraction con-

Table III—Asymptotic power density drop-off for circular distributions

Circular Aperture Distribution	Asymptotic Power Density Drop-Off
Uniform	u^{-3}
$1 - (\rho/a)^2$	u^{-5}
$[1 - (\rho/a)^2]^2$	u^{-7}
$[1 - (\pi/a)^2]^3$	u^{-9}
Circular Taylor	u^{-3}

tribution resulting from saddle-point integration, which applies principally to the main beam (see, for example, Ref. 12).

The radiation pattern of a planar aperture with rectangular separable distributions (rule 3 in Table I) is a product of the principal plane patterns. Polar separable distributions generate patterns with drop-off rate $u^{-n-(1/2)}$ by integrating the Hankel transform[13] by parts and using asymptotic expressions for the Bessel functions. Representative circular distributions are listed in Table III.[14] Discrete element construction of the aperture distribution adds grating lobes to the antenna pattern when the elements are periodically displaced. The grating lobes are isolated, however, and their location can be predicted from the array structure.

A wedge diffraction pattern is a product of axial and cross patterns, with the latter culminating at the shadow boundaries of the incident and reflected illuminations and decaying from it as $(\sin \gamma/2)^{-1}$ for a thin wedge or as $(\sin 3\gamma/2)^{-1}$ for a right-angle wedge,[15] γ being the angle from the shadow boundary.

Diffraction by strips and cylinders is similarly a product of axial and cross patterns, where Snell reflection rules apply to the axial pattern. The diffraction pattern thus forms a cone around the axis, azimuthally and axially weighted by the respective pattern behavior.

2.3 Reconstruction of the antenna 3D radiation envelope approximation

The above survey shows simple pattern behavior for elemental radiators when represented in their natural coordinate systems. The generic form

$$F(u)(\text{dB}) = a - b \log_{10} u \tag{4}$$

may be used on each of the principal axes of the pattern of a separable distribution or edge diffraction and on representative radial cuts for a nonseparable distribution where azimuthal interpolation functions can close the gap. Paraboloids, circular or elliptical, are used to match the peak regions.

Contributions to the antenna radiation pattern come from the illumination of the aperture and its edges, diffraction by the feed and structural members, and the weather cover. All these can be classified by the categories surveyed in the previous section, and the characteristic pattern of each can be traced on the 3D antenna pattern in regions where it dominates. These traces are easiest to identify on the sin θ, ϕ polar plot of the antenna pattern, pivoted around the boresight, where they take elliptical shapes. For instance, an edge slanted by an angle α from boresight (z axis) in a plane slanted by β from the xz plane, diffracts the outgoing wave on a cone, the trace of which is an ellipse with axes

$$a = \sin \alpha$$
$$b = (1/2) \sin 2\alpha \tag{5}$$

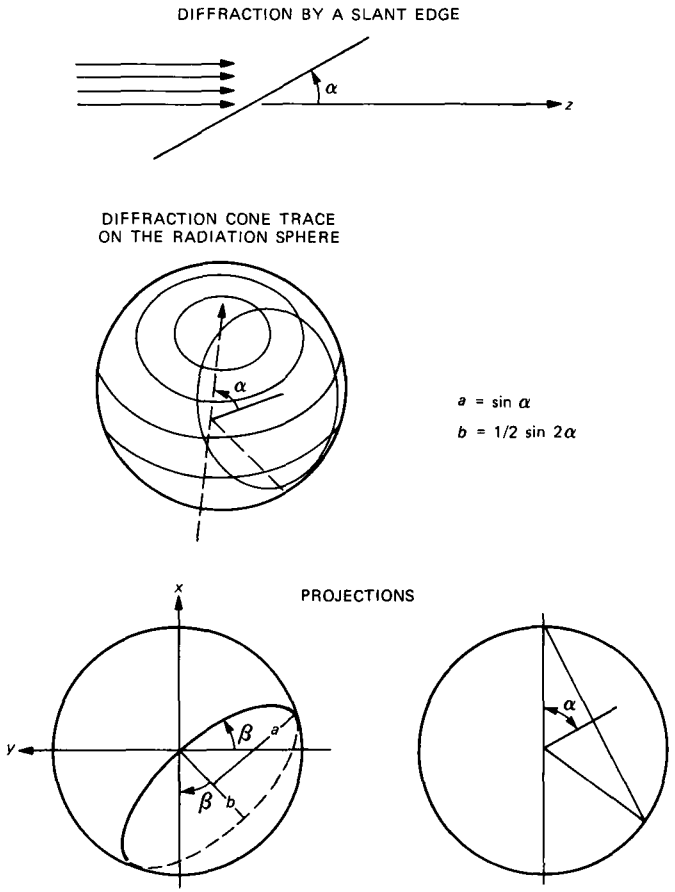

Fig. 2—Projections of the edge diffraction cone.

tangent to a line through the boresight forming an angle β with the y axis (see Fig. 2).

Once skeleton shape matching is obtained, parameters of eq. (4) are adjusted to match the envelope of each contributor in its natural coordinate system. The partial patterns are then retransformed to the antenna coordinate system where final patch up might be required in transition regions.

The desired application of the radiation envelope approximation should determine the coordinates of representation and the transformation formulas. In analyzing scattering interference in terrestrial transmission, for instance, the azimuth (AZ)-elevation (EL) coordinate system blends with the computations of the model much better than θ, ϕ coordinates, and the transformations and approximations are best done directly in that representation (see Fig. 1).

III. THE PYRAMIDAL HORN-REFLECTOR ANTENNA PATTERN

The PHR antenna is extensively used in terrestrial microwave links (see Fig. 3). The measured data of the frontal hemisphere of its 3D radiation pattern at 4 GHz consists of 91 ϕ cuts made every 1° with a sampling rate of 0.08° totaling about 200,000 measured points.[9] The sin θ, ϕ polar plot of its radiation distribution for horizontal polariza-

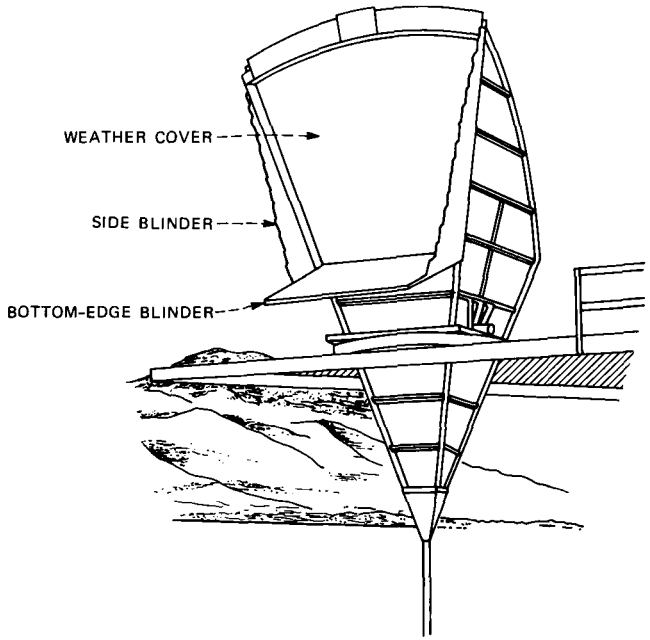

Fig. 3—The AT&T pyramidal horn-reflector antenna.

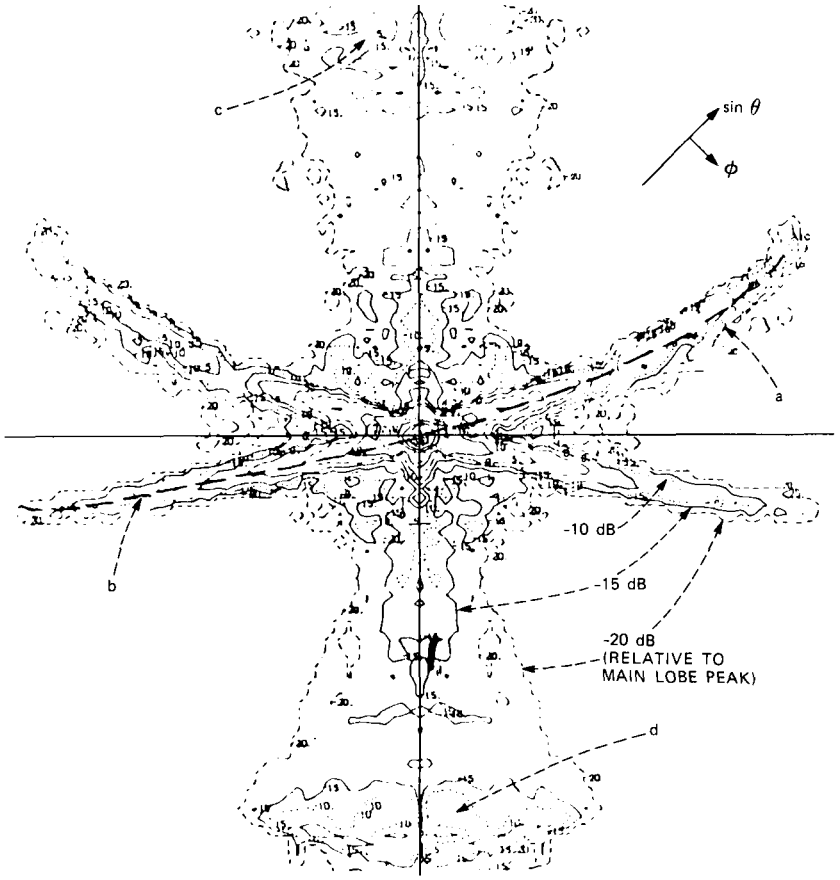

Fig. 4—Radiation pattern for the pyramidal horn-reflector antenna of Fig. 3 in sin θ, ϕ coordinates at 3900 MHz, horizontal polarization.

tion is shown in Fig. 4, truncated at 60 dB below the main beam peak, while the accompanying 3D pattern is shown in Fig. 5 in AZ-EL coordinates. The trace a in Fig. 4 could be matched to an ellipse with $\alpha = 14.5°$, $\beta = 14.5°$ and identified as side edge diffraction. The trace b, on the other hand, matches an ellipse with $\alpha = 3.6°$, $\beta = 14.5°$ corresponding to the side blinder (see Fig. 3).[16] A closer look at the side blinder attachment detail shows a step at the aperture edge, allowing for the aperture edge diffraction to dominate on one side and to be shadowed by the side blinder on the other. The large diffused lobe at d is due to reflection by the weather cover emerging down after a second bounce from the reflector (see Fig. 6), while the one at c is a spillover of the horn field illuminating the top edge of the reflector. The flare of the side-lobe ridge at the top and at the bottom is attributed to the curved top edge of the aperture.

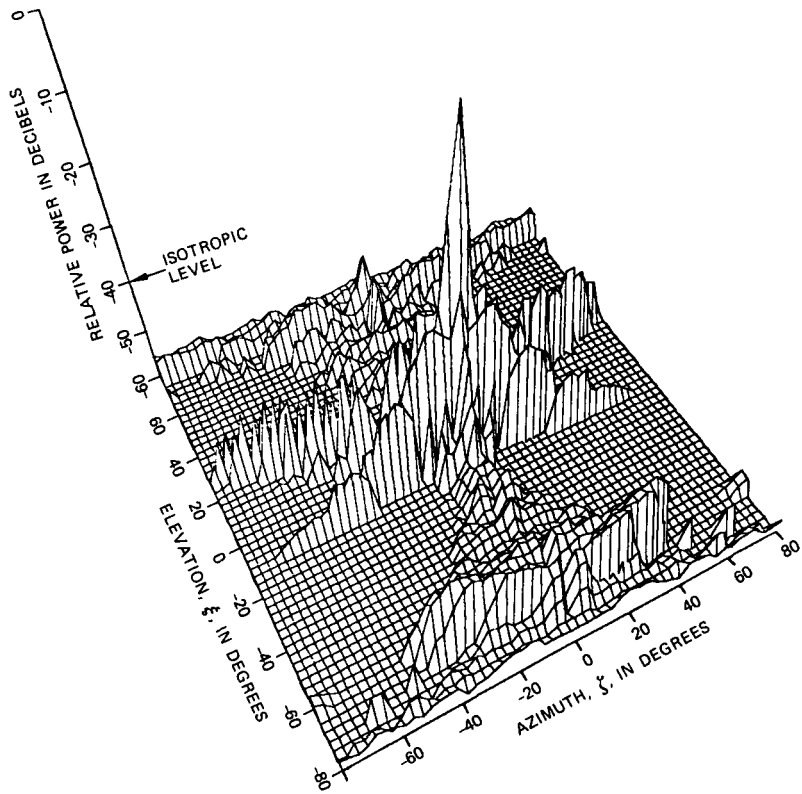

Fig. 5—Radiation pattern for the pyramidal horn-reflector antenna in AZ-EL coordinates at 3900 MHz, horizontal polarization.

The aperture field of the PHR antenna has the TE_{10}-mode distribution prevailing in the pyramidal horn, blown up by the reflector. The horizontally polarized field strongly illuminates the side walls but is much weaker at the upper and bottom edges. The case is reversed with vertical polarization as shown in Figs. 7 and 8; the side wall diffraction is highly suppressed, while that of the top and bottom edges is very strong at the center and decays to the sides. The spillover lobe, c, is much stronger, but the window lobe, d, is similar to that of the horizontal polarization.

IV. THE RADIATION ENVELOPE APPROXIMATION FOR THE PHR ANTENNA

The contributors to the radiation pattern, identified by examination of both the pattern and the antenna, are aperture illumination taper, top edge (curved), bottom edge, side edges (slanted $\alpha = 14.5°$, $\beta =$

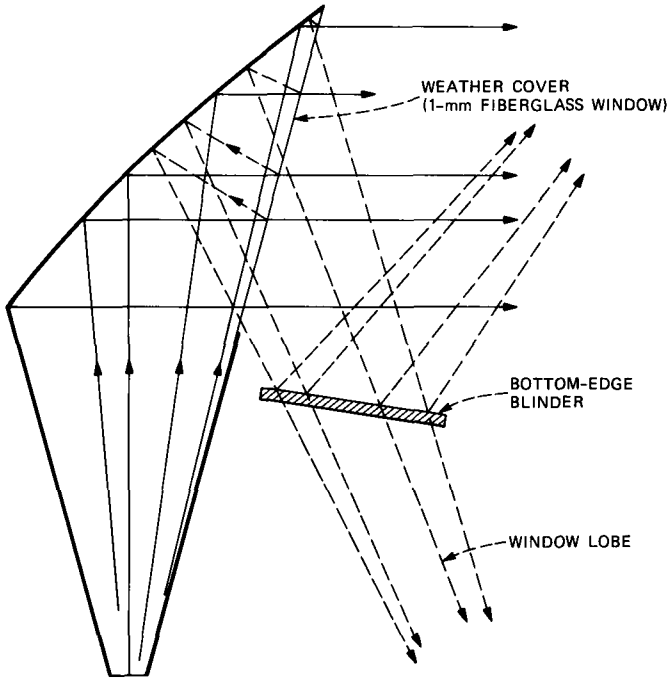

Fig. 6—Pyramidal horn-reflector antenna with bottom-edge blinder and window lobe.

14.5°), side blinders (slanted $\alpha = 3.6°$, $\beta = 14.5°$), weather cover (window lobe), top-edge spillover, and bottom-edge blinder (optional). Each of these contributions is approximated by the following generic function in the peak regions:

$$g = g_{\max} - K_u(u - u_0)^2 - K_v(v - v_0)^2, \tag{6}$$

where $g_{\max}$ is the peak level in decibels below the main beam peak, u and v are the local principal plane coordinates [see eq. (1)] for each contributor, and K_u, K_v are the parabolic coefficients to be matched. In the fall-off regions,

$$g = a_u + a_v - b_u \log_{10} u - b_v \log_{10} v \tag{7}$$

supplies the envelope, with a_u, a_v, b_u, b_v coefficients to be matched. The local coordinate systems are then transformed to the antenna sin AZ, sin EL coordinate system for preserving computational economy in the repeated transformations between the antenna and the scattering model[1] coordinates. Such a simplification is made possible by the fact that the antenna boresight is almost horizontal and its azimuthal plane aligns with that of the scattering model to enough accuracy. The

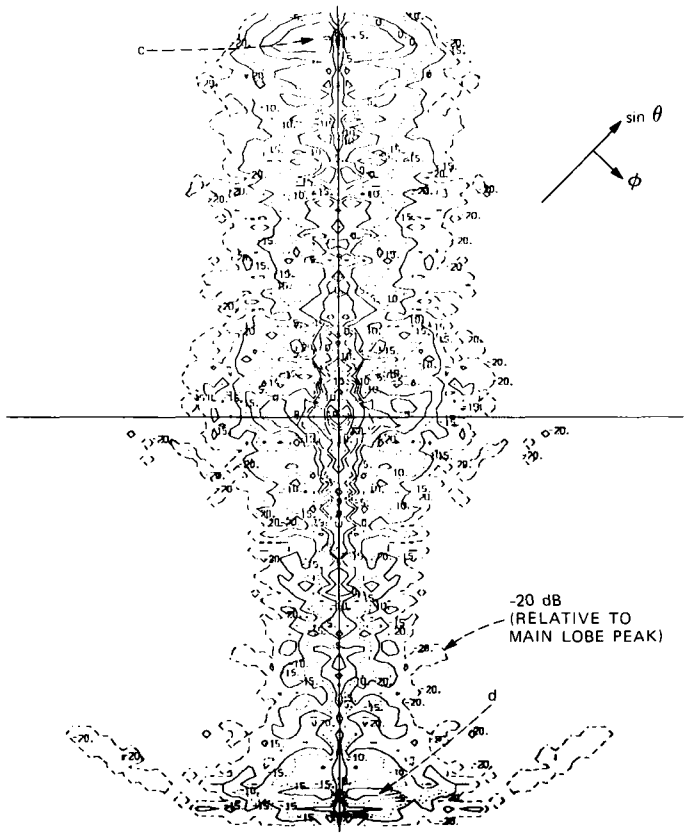

Fig. 7—Radiation pattern for the pyramidal horn-reflector antenna in sin θ, ϕ coordinates, vertical polarization.

sin AZ, sin EL coordinate system is presented in Fig. 1 and is related to the spherical coordinates via

$$\sin \text{EL} = \sin \theta \sin \phi = u$$

$$\sin \text{AZ} = \sin \theta \cos \phi / \sqrt{1 - \sin^2 \theta \sin^2 \phi}$$

and

$$\cos \theta = \cos \text{AZ} \cos \text{EL}$$

$$\sin \phi = \sin \text{EL} / \sqrt{1 - \cos^2 \text{AZ} \cos^2 \text{EL}}.$$

The top edge contribution is flared to ±15° by scaling the AZ coordinate input to eq. (7).

The partial contributions to the radiation envelope thus obtained are drawn in Figs. 9 through 12 and 14 through 17 for horizontal and vertical polarizations, respectively. The overall radiation envelopes,

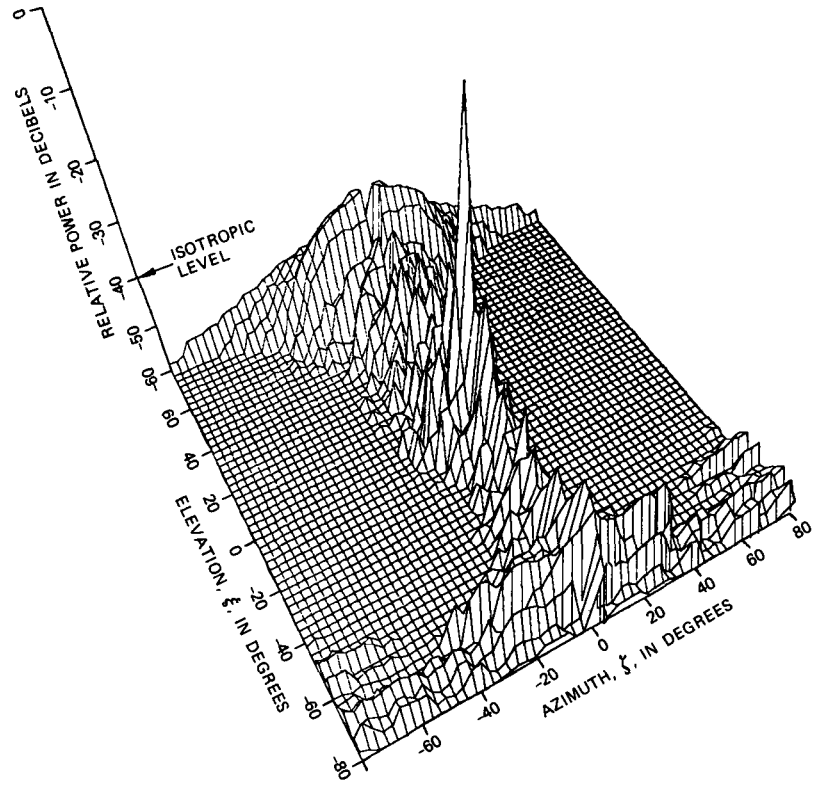

Fig. 8—Radiation pattern for the pyramidal horn-reflector antenna, vertical polarization.

drawn in Figs. 13 and 18 for these polarizations, respectively, are then represented by the largest partial contribution at every point, all the rest being ignored. Note that the three contributions aperture illumination taper, top edge, and bottom edge have been combined into one. The PHR antenna radiation envelope can, therefore, be well approximated by single functions of the type (6) or (7) in every region characterized by their respective coefficients. The total number of constants used by the program for each polarization is 36, only four or five of which are used in any individual function. Also, transformations using eq. (5) are required for the side edge and side blinder contributions.

V. SUMMARY

A procedure was described by which a simple and computationally economical mathematical model can be constructed to approximate

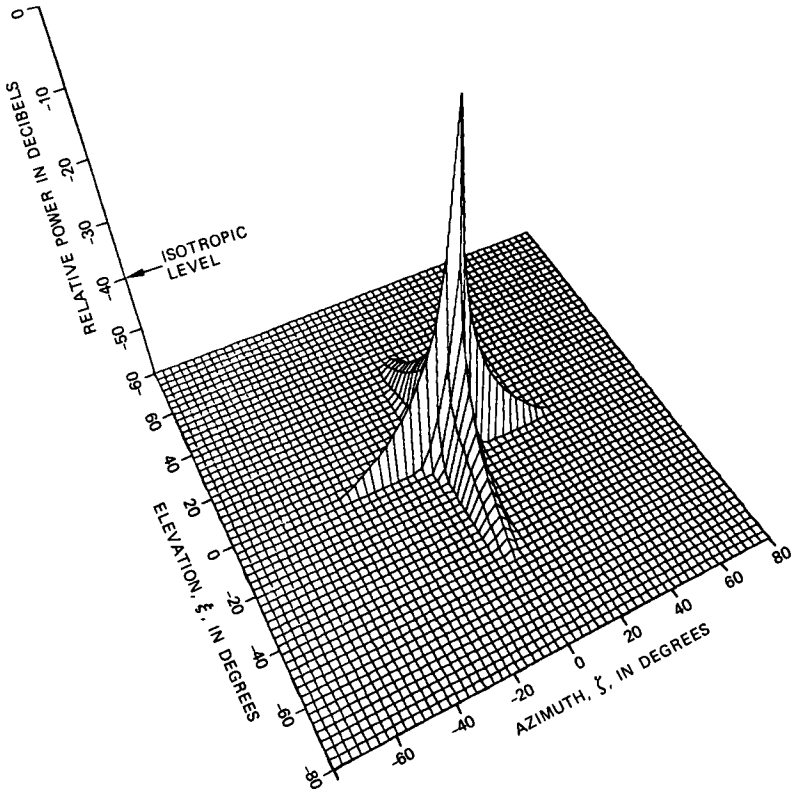

Fig. 9—Partial radiation envelope due to aperture and top and bottom edges, horizontal polarization.

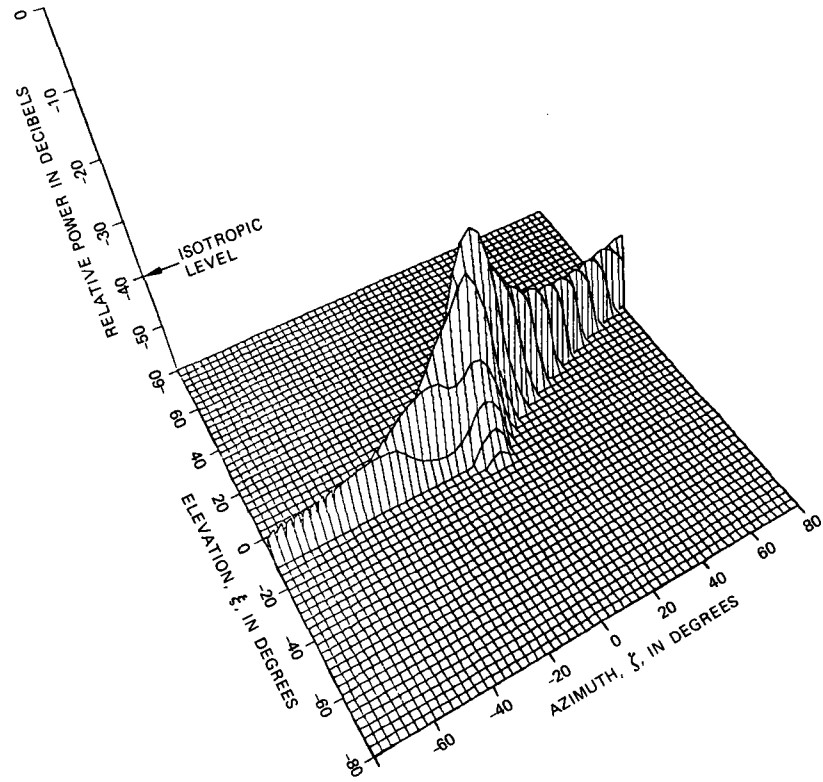

Fig. 10—Partial radiation envelope due to right edge, horizontal polarization.

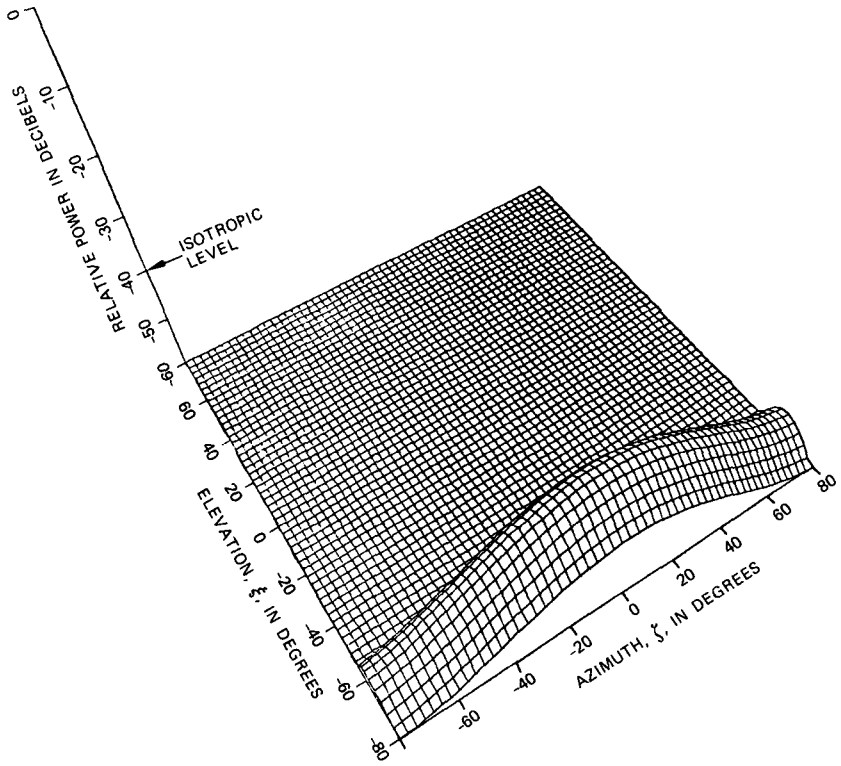

Fig. 11—Partial radiation envelope due to window lobe, horizontal polarization.

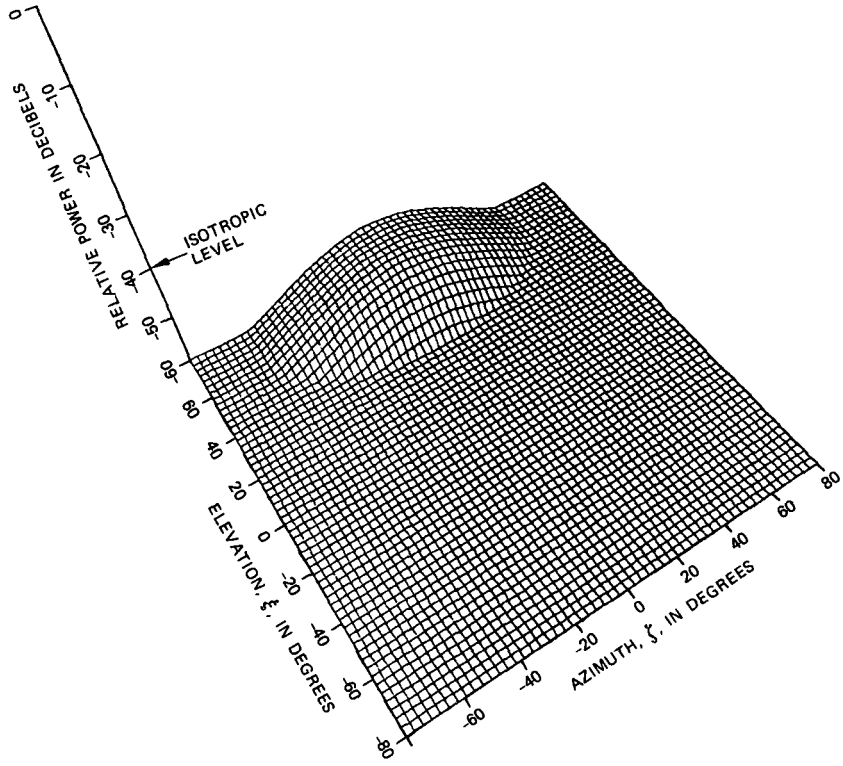

Fig. 12—Partial radiation envelope due to spillover, horizontal polarization.

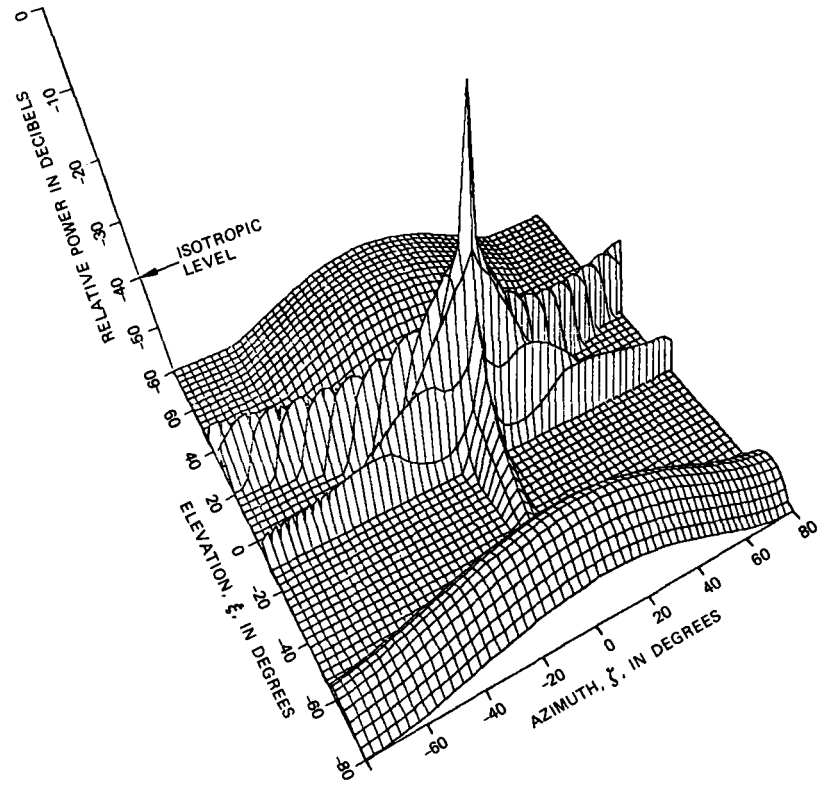

Fig. 13—Overall radiation envelope for the pyramidal horn-reflector antenna, horizontal polarization.

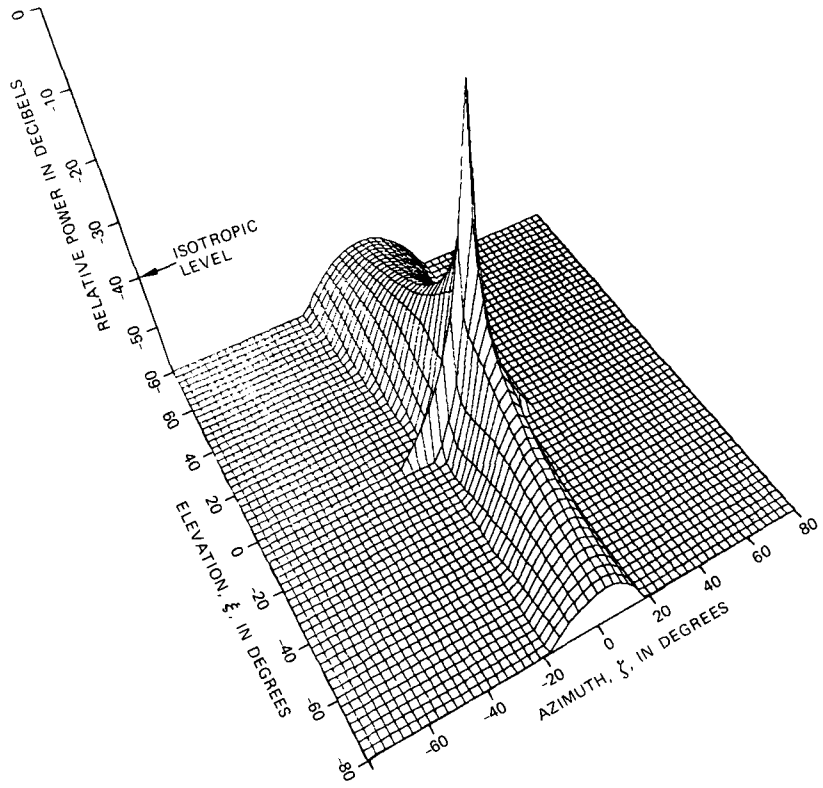

Fig. 14—Partial radiation envelope due to aperture and top and bottom edges, vertical polarization.

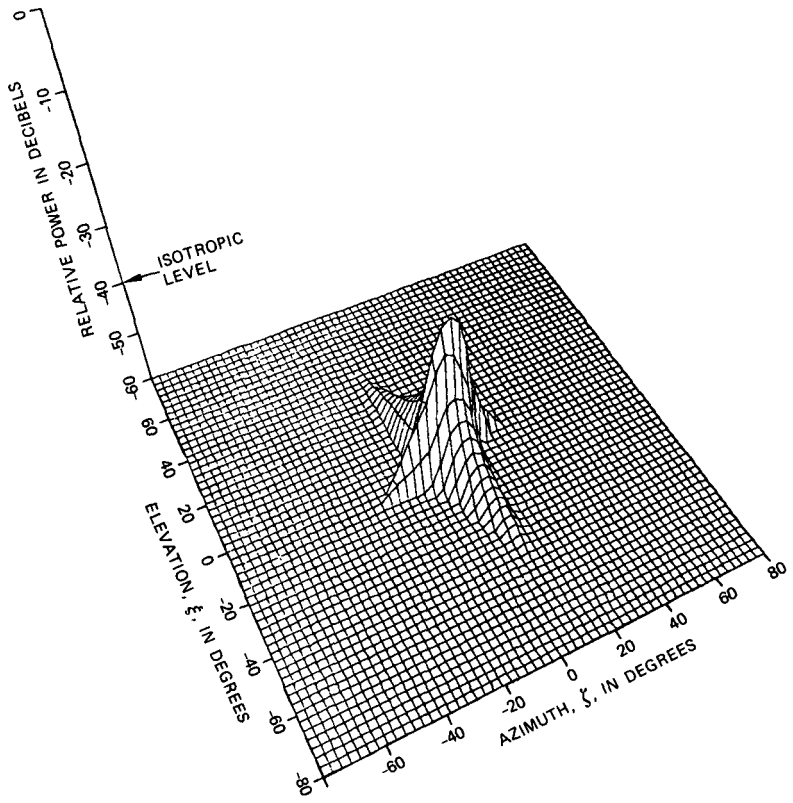

Fig. 15—Partial radiation envelope due to right edge, vertical polarization.

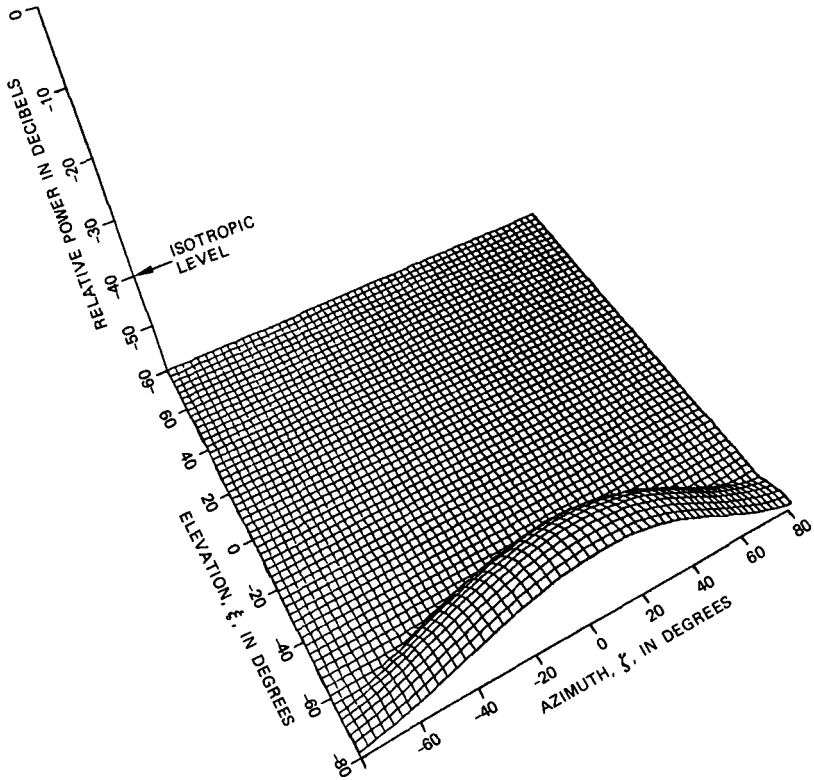

Fig. 16—Partial radiation envelope due to window lobe, vertical polarization.

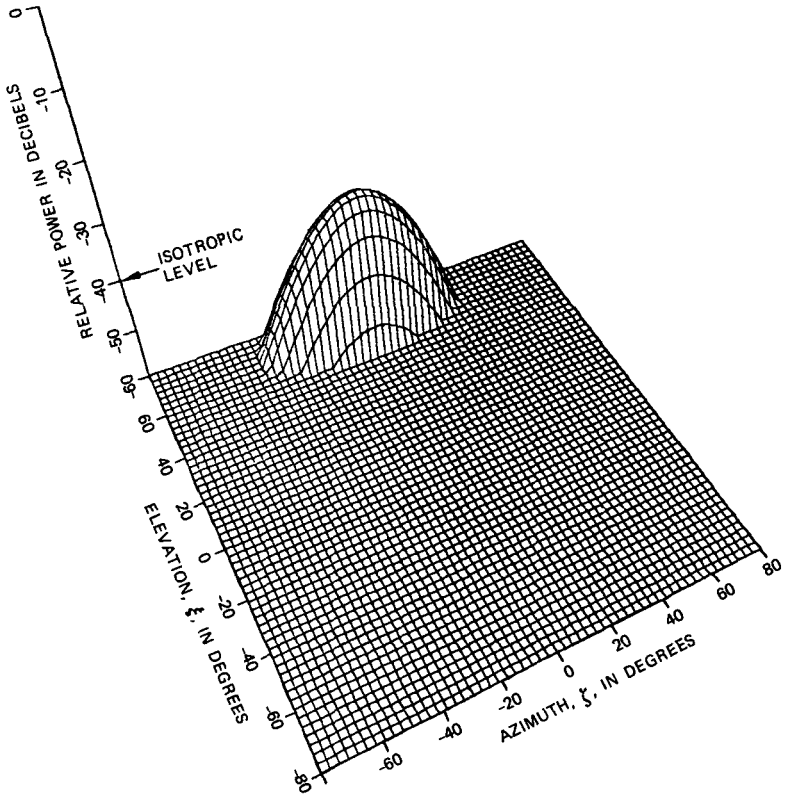

Fig. 17—Partial radiation envelope due to spillover, vertical polarization.

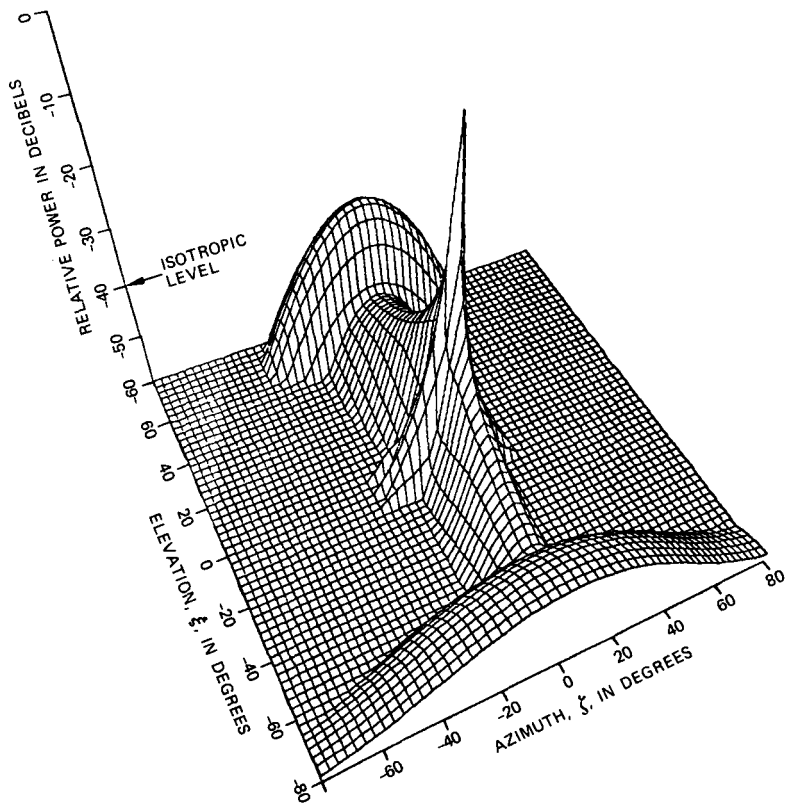

Fig. 18—Overall radiation envelope for the pyramidal horn-reflector antenna, vertical polarization.

the 3D radiation envelope of directive antennas by making proper use of the salient antenna features. Accuracy is a parameter in such a model. Test computations of carrier-to-interference ratios executed by using this model versus the measured 3D pattern in the terrain scattering interference model[1] agreed to better than 3 dB in all cases.

VI. ACKNOWLEDGMENTS

The author is grateful to Mr. W. A. Gianopoulos for his excellent programming work and to his colleagues Messrs. A. J. Giger, H. C. Wang, and P. E. Butzien for their comments and editing work.

REFERENCES

1. A. J. Giger and J. Shapira, "Interference Caused by Ground Scattering in Terrestrial Microwave Radio Systems," ICC '83 Conf. Rec. (June 1983), pp. 1254–61.
2. J. Shapira, "Sampling and Processing in Antenna Pattern Measurements," Proc. 11th Convention of Electrical and Electronic Engineers in Israel (October 1979), IEEE Publication 79CH1566-9, p. B2-5.

3. O. M. Bucci et al., "Use of Sampling Functions for the Analysis of Radiating Structures," Final Report to ESTEC Contract N.4380/80/NL/DS, 1981.
4. International Radio Consultative Committee (CCIR), 13th Plenary Assembly, Radiation Diagrams of Antennas for Earth Stations in the Fixed Satellite Service for Use in Interference Studies, Rep. 391-4, Vol. IV, Int. Telecommun. Union, Geneva, Switzerland.
5. W. Kuebler, "A Procedure for Estimating the Power Pattern of a Narrow-Beam Antenna," IEEE Trans., *EMC-23*, No. 2 (May 1981), pp. 100–3.
6. H. T. Friis, "Microwave Repeater Research," B.S.T.J., *27*, No. 2 (April 1948), pp. 183–246.
7. J. Shapira, "Simple Representations of Antenna Spatial Radiation Patterns," Dig. IEEE, *AP-S*, 1983 Int. Symp., May 1983, pp. 112–5.
8. J. N. Hines, Tingye Li, and R. H. Turrin, "The Electrical Characteristics of the Conical Horn-Reflector Antenna," B.S.T.J., *42*, No. 4, Part 2 (July 1963), pp. 1187–211.
9. P. E. Butzien, "Three-Dimensional Radiation Characteristics of a Pyramidal Horn-Reflector Antenna," B.S.T.J., *60*, No. 6 (July–August 1981), pp. 913–21.
10. E. V. Jull, "Aperture Antennas and Diffraction Theory," Peter Peregrinus Ltd., 1981, pp. 68–73.
11. F. J. Harris, "On the Use of Windows for Harmonic Analysis With the Discrete Fourier Transform," Proc. IEEE, *66*, No. 1 (January 1978), pp. 51–83.
12. L. B. Felsen and N. Marcuvitz, *Radiation and Scattering of Waves*, Englewood Cliffs, N.J.: Prentice-Hall, 1973.
13. A. Papoulis, *Systems and Transforms With Applications in Optics*, New York: McGraw-Hill, 1968, p. 163.
14. W. L. Stutzman and G. A. Thiele, *Antenna Theory and Design*, New York: Wiley, 1981.
15. R. G. Kouyoumjian, *The Geometric Theory of Diffraction and Its Applications in Numerical and Asymptotic Techniques in Electromagnetics*, New York: Springer-Verlag, 1975.
16. D. T. Thomas, "Design of Multiple-Edge Blinders for Large Horn-Reflector Antennas," IEEE Trans. Ant. Propag., *AP-21*, No. 2 (March 1973), pp. 53–158.

AUTHOR

Joseph Shapira, B.Sc. and M.Sc. (Electrical Engineering), Technion–Israel Institute of Technology, in 1961 and 1976, respectively; Ph.D. (Electrophysics), 1973, Polytechnic Institute of New York; Rafael–Armament Development Authority of Israel, 1963–1980, 1981–1982, 1983—; Electro-optics Industries of Israel, 1980–1981; Bell Laboratories, 1982–1983. During his first years with Rafael, Mr. Shapira founded and headed the Electromagnetics Department, encompassing research and development in antennas, arrays, radomes, propagation, target characteristics and electromagnetic compatibility. In 1979 he was appointed advisor on electromagnetic systems to the Director of Rafael. Later that year he was assigned Special Assistant to the Chief of Research and Development of the Israeli Ministry of Defense, where he directed reviews and planning of high technology major projects in radar, fire control, and communication systems. In 1980 he became the manager of the Optronics Systems Operation in the Electro-optics Industries of Israel. In 1981 he returned to Rafael as a Research Fellow. From 1982 to 1983 he was with Bell Laboratories, on a Sabbatical leave from Rafael, where he was engaged in terrain scattering research. He is now Deputy Director of the Guidance Division Rafael. Mr. Shapira is also affiliated with the Technion, Haifa, as a part-time Associate Professor in the Electrical Engineering Faculty. His areas of interest are electromagnetic engineering and electromagnetic compatibility. He won the IEEE antenna and Propagation Society Best Paper Award in 1974 as a coauthor of "Ray Analysis of Conformal Antenna Arrays." In 1980 he

was awarded the A. D. Bergman Prize (presented by the President of Israel) for scientific and technical achievements in electromagnetic engineering, and his contributions to Rafael's technological capabilities. In 1981 Mr. Shapira was nominated the President of The Israel National Committee for Radio Science, and he was nominated to the delegation to the International Union of Radio Science. Senior member, IEEE.